Available online at www.sciencedirect.com
SCIENCE DIRECT
Journal of Solid State Chemistry 179 (2006) 873–882
JOURNAL OF SOLID STATE CHEMISTRY
www.elsevier.com/locate/jssc

Formation and performances of porous $InVO_4$ films

Shicheng Zhang[a,b], Chuan Zhang[a], Haipeng Yang[a], Yongfa Zhu[a,*]

[a]*Department of Chemistry, Tsinghua University, Beijing, 100084, PR China*
[b]*Department of Environmental Science and Technology, Fudan University, Shanghai 200433, PR China*

Received 14 July 2005; received in revised form 10 November 2005; accepted 9 December 2005
Available online 20 January 2006

Abstract

Porous complex oxide films consisting of preferentially orientated orthorhombic phase of $InVO_4$ have been prepared using a novel simple method by pyrolysis of amorphous complex precursor. The formation and controlling of porous $InVO_4$ films can be easily obtained by modifying the calcination temperature. The pure orthorhombic $InVO_4$ phase can be obtained at a relatively lower temperature (500 °C), and the films are preferential orientation of the (200) face parallel to the substrate. The phase separation mechanism was suggested for the formation of porous films. Under visible light irradiation ($\lambda > 400$ nm), porous $InVO_4$ films have shown the photocatalytic activity for photodegradation of gaseous formaldehyde, and can generate photocurrent. The electrochemical properties of the films with different crystal structure and pore structure were also investigated.

Keywords: $InVO_4$; Dip-coating; Porous films; Photocatalytic activity; Visible light; Electrochemical properties

1. Introduction

Mesoporous and macroporous films have attracted great interest for their potential uses in catalysis [1], high selective adsorbents, photoelectrodes [2–4], photocatalysts [5,6], gas sensors [7,8], electrochromic materials [9,10], lithium ion batteries [11,12], and so on. Different methods for the synthesis of mesoporous and macroporous films have been developed during the past several decades [13,14]. The most popular methods are the template methods, using the surfactants [15,16], block copolymer [17–19], or colloidal sphere [20–22] as the templates. By using the colloidal sphere arrays as the template and filling the void spaces with nanoparticles, the ordered macroporous materials can be obtained. This method offers the great advantage of incorporating specific nanoparticles of desirable crystalline phases into the wall structure of the macroporous framework. By using the surfactants and the block copolymer as the templates, many mesoporous films have been obtained from the hydrolysis of the metal alkoxides, such as SiO_2, TiO_2, ZrO_2, ZrP, and so on. For the limitation of the metal alkoxides, finding a simple method for the preparation of porous films from low cost raw materials is still a challenge.

$InVO_4$ has attracted interest for its special electrochemical and photocatalytic properties. $InVO_4$ belongs to the family of orthovanadates, oxides with attractive properties as Li insertion electrodes, and is proposed as an anode material for lithium rechargeable batteries [23], and electrochromic windows due to their transparency [24]. Very recently, calculated by first principles calculations, and supported by experiments, $InVO_4$ is a promising photocatalyst that is able to induce hydrolysis of water molecules under visible light irradiation [25–27]. The electronic structures of the thin films of $InVO_4$ have also been calculated by first principles calculations [28], and it is found that the band gap of $InVO_4$ films seems to be very sensitive to the V environment around O atom. So, it is very interesting and essential to prepare the $InVO_4$ films on the transparent conducting substrates. $InVO_4$ films have been prepared by using the sol–gel route from V-oxoisopropoxide and In-nitrate precursors by the dip-coating technique [29,30]. Thin films of mixed In/V oxides have also been obtained by reactive RF sputtering [31]. But the preparation of porous films of $InVO_4$ has not been reported.

*Corresponding author.
E-mail addresses: zhangsc@fudan.edu.cn (S. Zhang), zhuyf@mail.tsinghua.edu.cn (Y. Zhu).

0022-4596/$ - see front matter © 2005 Elsevier Inc. All rights reserved.
doi:10.1016/j.jssc.2005.12.021

Here, we report a new simple method for the preparation of porous $InVO_4$ films by direct pyrolysis of an amorphous complex precursor. This kind of method has been used in the preparation of complex oxide powders or dense films [32–35]. But there are still no reports on the preparation of porous films. The homogenous amorphous complex precursor is produced by the complexation between diethylenetriaminepentaacetic acid (DTPA) and low cost metal oxides or salts. The high viscosity of the precursor makes it suitable for the preparation of complex oxide films by the dip-coating or spin-coating technique. The formation mechanism was investigated by using the TEM, FE-SEM, XRD, Raman, FTIR, and XPS. The pore size was modified easily by changing the calcination temperature. The optical, electrochemical, photocatalytic, and photoelectrochemical properties of porous $InVO_4$ films were also discussed.

2. Experimental section

2.1. Preparation of porous $InVO_4$ films

The porous $InVO_4$ films were prepared by using the dip-coating technique from amorphous complex precursor. The complex precursor of $InV(DTPA)_{1.6}$ solution was synthesized by using DTPA as a ligand. All chemicals used were of analytical grade and were purchased from Beijing Chemical Factory (China). The substrates were ITO glasses, which were purchased from China Southern Glass Co. Ltd., with a thickness of ITO of 135 nm and a sheet resistance of $15\,\Omega/\square$.

Scheme 1 described the preparation process. A typical synthesis procedure was shown below. A 0.009 mol In_2O_3 powder was dissolved in 5 mL hot concentrated HCl solution. Then, 10 mL stronger ammonia water was added to the solution to get the $In(OH)_3$ deposit. Subsequently, the deposit was centrifuged and washed several times till the pH value of the supernatant fluid approached 7. The $InV(DTPA)_{1.6}$ aqueous solution was obtained by the dissolution of the deposit and 0.009 mol V_2O_5 powder in H_5DTPA solution (0.0396 mol in 100 mL de-ionized water) at 80 °C under vigorous stirring. Finally, the $InV(DTPA)_{1.6}$ aqueous solution was evaporated and concentrated to 50 mL to get the precursor for dip-coating. For the detection of TG-DTA, the solution was vaporized slowly at 80 °C to become a piece of blue transparent glass-like material, and then it was grinded to a powder sample.

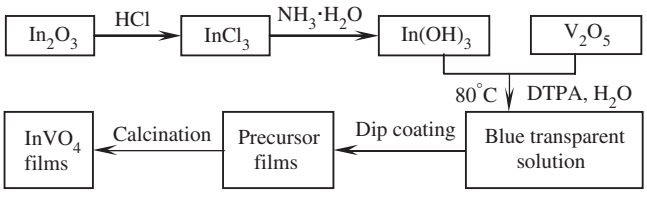

Scheme 1. Process flowsheet for preparation of $InVO_4$ films.

Before dip-coating, the ITO glasses were first cleaned by scrubbing in detergent and then in distilled water. Then they were immersed sequentially in ultrasonic baths of ethanol and acetone, each for about 15 min. Then they were blow dried in a clean hood. Finally, each ITO plate was exposed to an 11 W mercury lamp in an enclosed housing for UV irradiation. The mercury lamp has a continuous emission spectrum starting at about 254 nm and with increasing intensities up to 190 nm.

The ITO glass substrates were dipped into the complex precursor for 2 min and the films were then deposited with a pulling velocity of 3 cm/min. After drying at 80 °C, the sample was heated to a certain temperature (400, 450, 500, and 550 °C) at 3 °C/min, and then calcined for 4 h in an air flow oven. The thickness of individual $InVO_4$ layers was ca. 100 nm; thicker films were obtained by consecutive dip-coating, each followed by annealing.

2.2. Samples characterization

The morphology of the samples was detected by using TEM and FE-SEM. TEM was performed by using a JEOL JEM-1200EX instrument with the accelerating voltage of the electron beam of 120 kV. FE-SEM was taken using a Hitachi S-450 electron microscope.

The crystal structure of the films was investigated by using XRD (Rigaku D/MAX-RB diffractometer) with Cu$K\alpha$ radiation and a scan rate of 4°/min.

Raman spectra were recorded on an RM 2000 microscopic confocal Raman spectrometer (Renishaw Company) with an excitation of 514 nm laser light at 0.5 mW, and were accumulated 12 times for 30 s each. The spectra were recorded with a charge coupled device (CCD) camera.

Thermogravimetric analysis (TGA) was carried out by using the Du Pont thermal analysis system (Dupont 1090B TGA 951 thermogravimetric Analyzer) with a heating rate 10°/min in air.

FTIR patterns were acquired from a Perkin–Elmer System 2000 infrared spectrometer.

The XPS analysis was measured on a PHI 5300 ESCA instrument using an Al Ka X-ray source at a power of 250 W. The pass energy of the analyzer was set at 35.75 eV and the base pressure of the analysis chamber was $<3\times10^{-9}$ Torr. The analyses were based on the following peaks: C1*s*, O1*s*, In3*d*, V2*p*, N1*s*. The binding energy scale was calibrated with respect to the C1*s* photopeak of hydrocarbon contamination fixed at 285.0 eV.

AES spectra were obtained using a PHI 610 scanning auger microscopy system. The beam voltage was 3.0 kV and the beam current was 0.5 μA. The electron beam was incident at an angle of 60° with respect to the specimen surface in order to make the sample surface perpendicular to the ion beam. During the depth profile analysis, the energy and beam current of the Ar ion beam were 3.0 keV and 6 μA, respectively. The beam diameter was 1 mm and the sputtering rate was approximately 30.0 nm/min for a thermally oxidized SiO_2 thin film.

Electrochemical and photoelectrochemical measurements were performed in a home-made three electrode quartz cells. Pt sheet was used as counter and Hg/Hg_2Cl_2/sat.KCl used as reference electrodes, while the working electrode was the thin film on ITO under investigation. The electrodes were immersed in a 1 mol L^{-1} solution of lithium perchlorate in propylene carbonate. The CV curves were recorded after 15 cycles at a scan rate of 50 mV s^{-1}. A 500 W Xe lamp was used as the excitation light source. The irradiated light intensity was measured with a power meter from the Institute of Electric Light Source (Beijing).

The visible light photocatalytic activities of $InVO_4$ films were valued by the decomposition of gaseous formaldehyde. The photoreactor used was a 250 ml cylindrical quartz vessel, which consisted of an inlet, an outlet, and a sample port. The $InVO_4$ film was tested in the vessel perpendicular to the light beam. The optical system for the photocatalytic reaction was composed of a 500 W Xe arc lamp and a cutoff filter ($\lambda > 400$ nm). The distance between the film and the light source was 20 cm, where the average light intensity was 31 mW cm^{-2}. The area of $InVO_4$ film was about 4 cm^2. The gaseous formaldehyde in the contaminated atmosphere was obtained by the vaporization of formaldehyde liquid using predetermined values of flow rate controlled by mass flow controllers. The mixture was then forced to flow through the photoreactor for 1 h. Then, the photoreactor was sealed and the photocatalytic reaction was started by turning on the lamp. Subsequently, the concentration of formaldehyde in the photoreactor, obtained by a gastight syringe from the sample port, was measured with an SP-502 gas chromatograph (GC) equipped with a flame ionization detector and a 2 m stainless steel column (GDX-403) at 373 K.

3. Results and discussions

3.1. Morphology and phase structure of the films

The morphologies of the precursor film and as-prepared films are shown in Fig. 1. The porous films were obtained by simply calcinating the precursor films and the pore size was easily adjusted by modifying the calcination temperature. The precursor film was very uniform. Under the calcination temperature of 400 °C, some white hillocks occurred, which was caused by the decomposition of hydrocarbon, amino-group organic compounds, and the

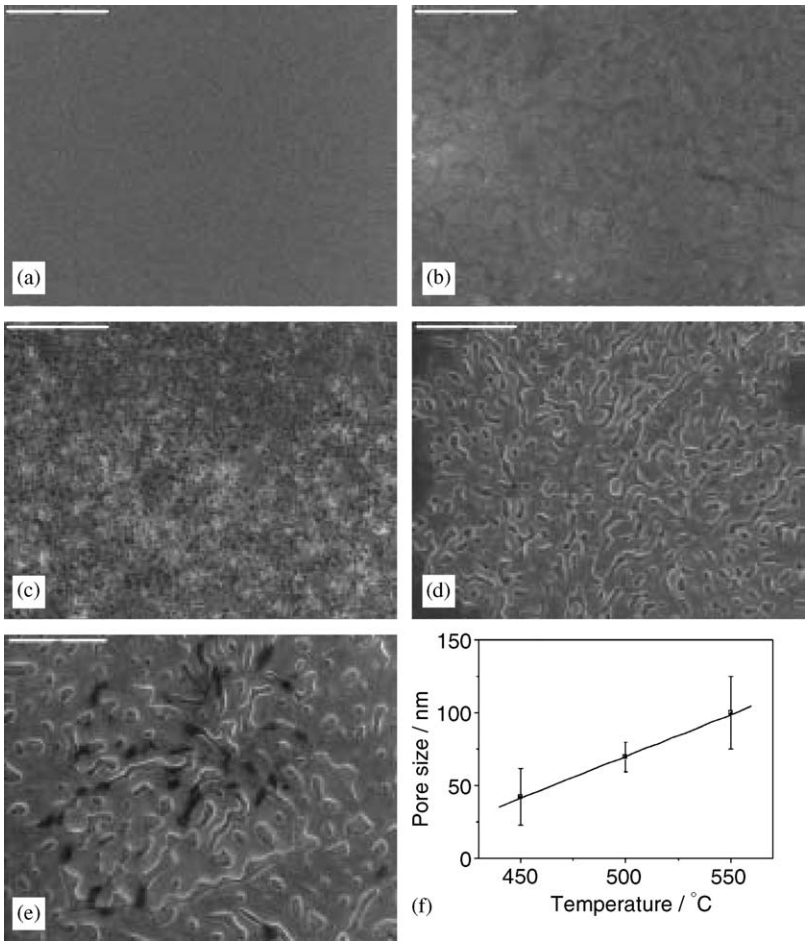

Fig. 1. SEM morphologies of precursor film (a) and as-prepared films obtained at different calcination temperatures: (b) 400 °C, (c) 450 °C, (d) 500 °C, (e) 550 °C. Scale bar: 500 nm. Also shows the average pore size vs. the calcination temperature with the error bars and the linear fitting (f).

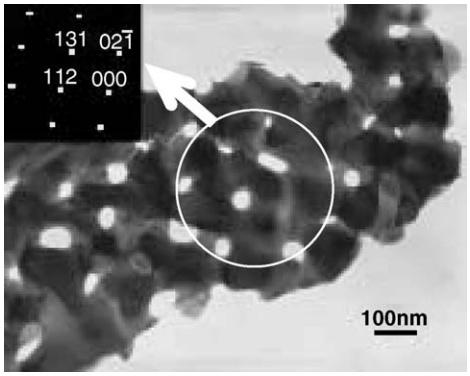

Fig. 2. TEM morphology of $InVO_4$ porous films obtained at 550 °C. Insert shows the ED pattern.

carboxyl indium group. From the surface, it is difficult to find the obvious pores. So the products (predominately CO_2) of the decomposition are trapped in the interior of the film, leading to the internal pores, which can be confirmed by the FTIR results in next section (Fig. 6b). At 450 °C, the pressure of the gas in the internal pores becomes high enough to break the pores and lead to the formation of the open pores on the surface of the film, with the average pore size of 40 nm, which was counted from the SEM images for about 100 pores. With the increase of the calcination temperature, the pore size increased linearly (Fig. 1f). From the SEM images, we can find that the film is free of cracks and the pore do not appear "ordered" in a long range. The TEM morphology and the selected electron diffraction (Fig. 2) of the $InVO_4$ films obtained under 550 °C show that the pores are in the interior of the single crystal.

The XRD patterns of the precursor film and as-prepared films are shown in Fig. 3. Only the In_2O_3 phase of ITO layer can be found in the patterns of the films obtained below 400 °C, and the broad peak between 20° and 30° two theta is amorphous silica in the glass substrate. Upon further increasing the annealing temperature, several Bragg peaks of orthorhombic $InVO_4$-III (JCPDF 48-0898) [36] appears in the XRD pattern, so that by 500 °C we obtain the X-ray signature of the orthorhombic $InVO_4$ phase, which is also supported by the Raman spectra (Fig. 4). The Raman spectra of the films obtained at 500 and 550 °C show the typical bands of $InVO_4$-III phase [37] at 915, 391, and 342 cm^{-1}, which match well with the Raman spectra of $InVO_4$-III powders.

From the literature, the $InVO_4$ with the pure orthorhombic phase was obtained above 600 °C, and only the low temperature phase monoclinic $InVO_4$ and no orthorhombic phase was obtained at 500 °C [23]. For the $InVO_4$ films prepared by using sol–gel method [29,30], the mixture of monoclinic and orthorhombic phases were obtained at a relatively low temperature (400 °C), but the pure high temperature phase had not been obtained. In the present work, the low temperature phase of $InVO_4$ (monoclinic phase) have not been obtained, but it gave a new method to

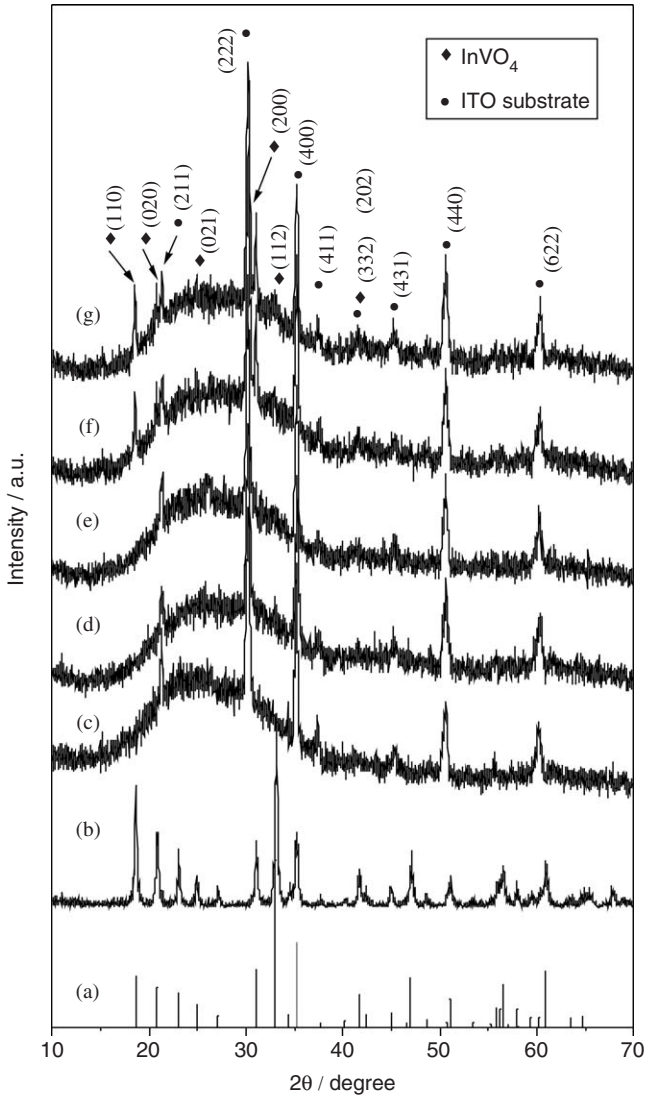

Fig. 3. XRD patterns of the precursor film (c) and the as-prepared films obtained under different calcination temperature: (d) 400 °C, (e) 450 °C, (f) 500 °C, (g) 550 °C. Also shows the standard patterns of orthorhombic $InVO_4$ (JCPDF 48-0898, (a) and the XRD pattern of $InVO_4$ powders (b).

prepare the pure, high temperature phase of $InVO_4$ (orthorhombic phase) at a relatively low temperature (500 °C).

From the XRD patterns of the films obtained under 500 and 550 °C (Figs. 3f and g), we can also find that the peak of (200) was enhanced, and the peak of (112) was weakened, which suggests preferential orientation of the (200) face of $InVO_4$ parallel to the substrate. One possible reason for the orientated growth of the $InVO_4$ films on the ITO substrate may be the heteroepitaxial growth.

Anyway, we have succeeded in the preparation of the crystallographically oriented porous films of $InVO_4$ by simply calcinating the precursor films, and the pore size was easily adjusted by modifying the calcination temperature.

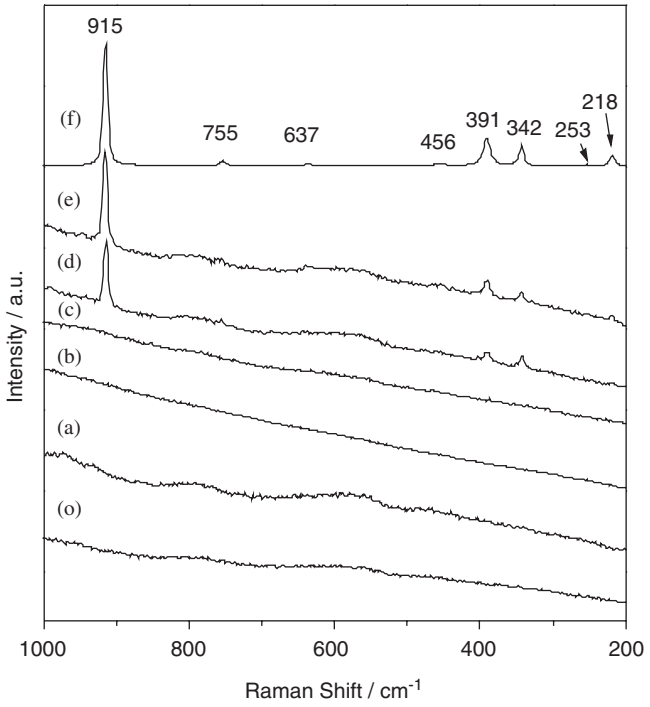

Fig. 4. Raman spectra of the precursor film (a) and the as-prepared films obtained under different calcination temperature: (b) 400 °C, (c) 450 °C, (d) 500 °C, and (e) 550 °C. Also shows the Raman spectrum of orthorhombic $InVO_4$ powders (f) and the ITO glass substrate (o).

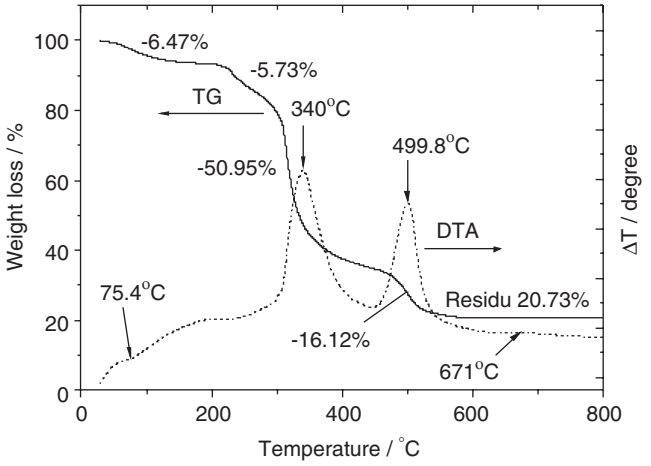

Fig. 5. TG and DTA measurements of $InV(DTPA)_{1.6} \cdot 4H_2O$ precursor. The DTA curve shows two obvious exothermic peaks, (E1) 340 °C and (E2) 499.8 °C. The TG curve shows four weight loss stages with the final temperature at (a) 130 °C, wt loss 6.47%; (b) 240 °C, wt loss 5.73%; (c) 410 °C, wt loss 50.95%; (d) 580 °C, wt loss 16.2%. And the residue is about 20.73%.

3.2. Formation process of porous $InVO_4$ films

In order to investigate the formation mechanism of the porous films, it is necessary to study the calcination process of the precursor films. Firstly, the decomposition process of the precursor powders was investigated by using TG and DTA spectra (Fig. 5). The TG curve indicated that the increase of temperature resulted in four different regions of weight loss. Based on the quantitative calculation of the weight loss in every region, the thermal decomposition processes can be distinguished as follows, which is similar to that of LaNi (DTPA) $\cdot 6H_2O$ for preparation of $LaNiO_3$ [35]. The weight loss region from 20 to 130 °C was caused by the loss of coordinated water. The region from 130 to 240 °C resulted from the decomposition of the organic group, including the decomposition of hydrocarbon, amino-group organic compounds. The region from 240 to 410 °C resulted from the decomposition of the carboxyl indium group, and the region from 410 to 580 °C resulted from the decomposition of the carboxyl vanadium group. All organic components could have been eliminated at 600 °C because there was no further weight loss.

On the DTA curve, one endothermic and three exothermic peaks were observed. The little endothermic peak at 75.4 °C was attributed to the loss of the coordinated water. The peak at 236 °C was produced by the burning of hydrocarbon and amino-group. The peak at 340 °C was produced by the decomposition of the carboxyl indium group. The peak at 499.8 °C corresponded to both exothermic contribution from the decomposition of the carboxyl vanadium group, and the formation of $InVO_4$ complicated oxide for the right tail of the peak, which can be confirmed by the XRD results that the crystalline $InVO_4$ was formed at 500 °C. The broad peak at 671 °C corresponded to allotropic transformations of $InVO_4$, which had been investigated in the literature [38]. The above results suggest that the decomposition of the organic components can be divided into two main stages: the stage below 400 °C and that above 400 °C, and the $InVO_4$ can be formed below 600 °C.

For investigation of the decomposition process of the precursor on ITO glass substrate, the precursor film and the films obtained at the transient temperature of two stages (400 °C) and the limiting temperature of ITO (550 °C) have been investigated by using FTIR (Fig. 6) and XPS (Fig. 7).

The bands of the FTIR spectra of the precursor film (Fig. 6a) at 3426, 3224, 3034, 2973, 2538, 1724, 1604, 1463, 1365, and 1094 cm^{-1} originated from the NH_2, C–N, C=O, C–O, and C–H bands. Above 400 °C, these bands almost completely disappeared. From the XPS results (Fig. 7 and Table 1), we can find that most of the organic components (C and N) were decomposed at 400 °C and completely decomposed at 550 °C. A part of the amounts of C and O in the films were caused by the contamination of CO_2 in the atmosphere. Compared with the decomposition of the precursor powders (from the TG-DTA results), the decomposition of the precursor film undergoes at a relatively lower temperature. The reason is that the precursor on the ITO glass is too little (the thickness of the film is only about 100 nm from the AES results) and has a big contact area with the air.

A carbon dioxide mode at 2333 cm^{-1} was observed in the FTIR spectra of $InVO_4$ (400 °C) films (Fig. 6b). Their

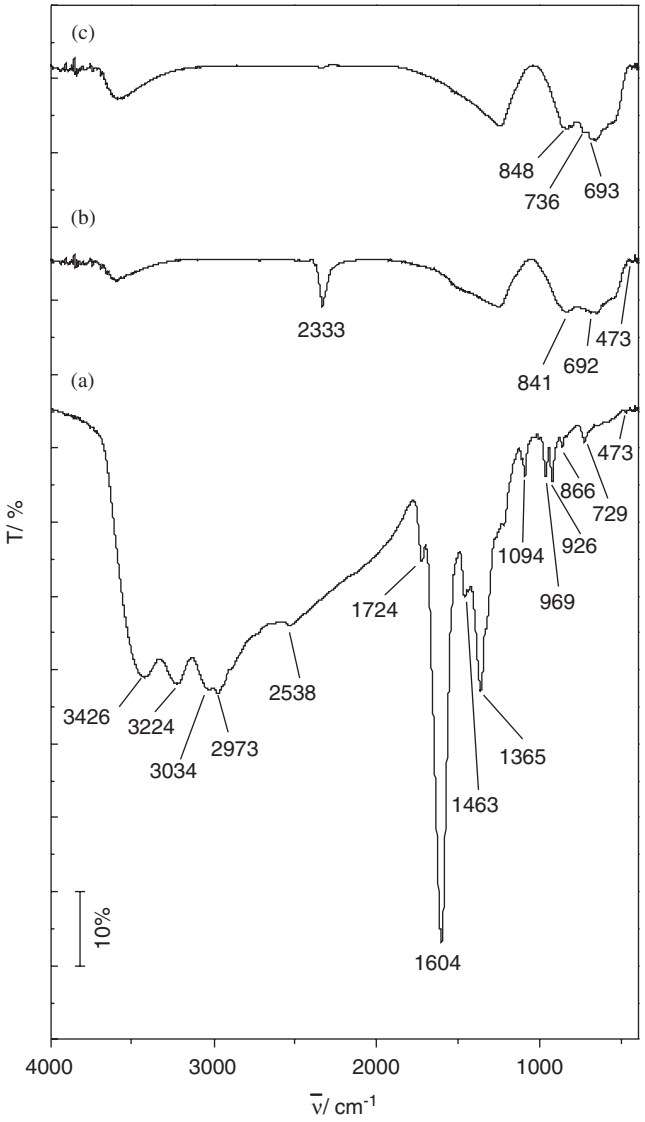

Fig. 6. Infrared spectra of the precursor films (a) and the $InVO_4$ films calcined at 400 °C (b) and 550 °C (c).

higher intensity in the spectra of the film suggests that CO_2 is trapped inside the porous structure of the film, which has also been found in the $InVO_4$ film prepared by the sol–gel technique [30]. Once the calcination temperature is increased, the pores were broken, leading to the liberation of CO_2 and the disappearance of the band of 2333 cm^{-1}. The detailed formation mechanism of the pores in the films will be discussed in the next section.

The 926 cm^{-1} band in the FTIR spectra of the precursor film was ascribed to the V^{4+}–O (vanadyl) stretching mode [30]. After calcination above 400 °C, this band disappeared. The same results can also be found from the XPS investigation. The V2*p* band of the precursor film is 514.8 eV, which belongs to a lower oxidation state of V (V^{4+}) [39]. After calcination above 400 °C, the V^{4+} was oxidized to V^{5+}, with the V2*p* band of 517.1 eV.

In the IR spectra of the precursor film and the films obtained at 400 °C, the band of 473 cm^{-1} is obvious, and it disappears in that of the film obtained at 550 °C (Fig. 6). From the literature, the 473 cm^{-1} band of the FTIR spectra was ascribed to the V–O–V scissoring vibration [40]. The crystal structure of the film obtained at 550 °C belongs to the orthorhombic phase (Figs. 3g and 4f), which is composed of two kinds of polyhedra: one is InO_6 octahedron and the other is VO_4 tetrahedron. The InO_6 octahedron connects to each other by sharing edge to form chains along the [001] direction, which were linked together by the VO_4 tetrahedra [27]. The VO_4 groups separated after crystallization [30]. So the disappearance of the band of 473 cm^{-1} was caused by the formation of the $InVO_4$ crystallized phase.

The binding energy of In3$d_{5/2}$ has been used to justify the crystallinity of the ITO film, i.e. the peaks at 444.08 and 445.24 eV are assigned to crystalline indium oxide (In_2O_3) and amorphous indium oxide, respectively [41]. Similar phenomenon has been found for the $InVO_4$ films. At 400 °C, the binding energy of In3$d_{5/2}$ at 444.8 eV was assigned to amorphous $InVO_4$, and at 550 °C, the binding energy of 444.2 was assigned to crystalline $InVO_4$ [39]. The structure of the $InVO_4$ films was also confirmed by the XRD and Raman results.

In summary, the calcination process of the precursor films can be divided into three stages: the decomposition of the organic components, the formation of the amorphous $InVO_4$ phase, and the formation of the crystalline $InVO_4$ phase.

3.3. Formation mechanism of porous $InVO_4$ films

Formation mechanism of the pores in $InVO_4$ films is similar to the phase separation mechanism put forward by Nakanishi [42] for the pore structure control of silica gel. The pores were formed by the CO_2 gas phase separation from the solid phase, which can be confirmed by the FTIR results. During the calcination process of the precursor film, the organic components decomposed into CO_2 firstly. Subsequently, the CO_2 gas separated from the solid phase, which led to the interior pores in the film.

If we suppose that the gas in the pores submits the perfect gas equation ($PV = nRT$, where P is pressure, V volume, n mole number, R perfect gas constant, and T temperature), with the increase of the calcination temperature, the pressure in the pores increases, which is the driving force for the enlarging of the pore and the merging of the solid phase. The increase of the volume of the pore will lead to the merger of adjacent pores to form a bigger one, and the decrease of the amount of the pores. Once the pore was big enough, the pore broke to form an open one. At the same time, the solid phase of $InVO_4$ also merged together into the big sheet with the pores imbedded. The amorphous phase of $InVO_4$ at lower calcination temperature is propitious to the merging of the solid phase. The schematic formation mechanism of the pore is shown in Fig. 8.

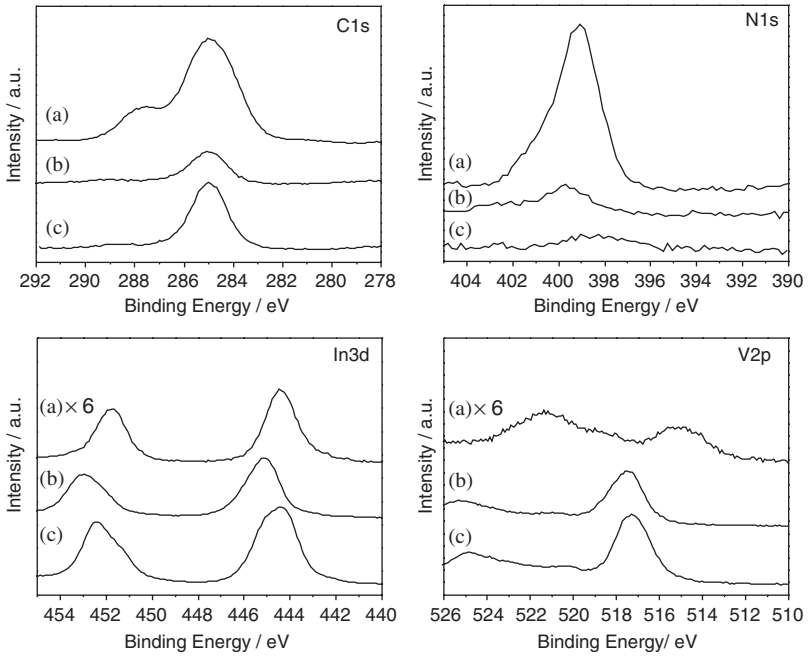

Fig. 7. X-ray photoelectron spectra of the precursor (a), the samples calcined at 400 °C for 4 h (b), and at 550 °C for 4 h (c).

Table 1
XPS binding energy values (eV) and atomic ratio for the reported compounds

Samples	In3$d_{5/2}$	V2$p_{3/2}$	In/V	O/V	C/V	N/V
Precursor	444.2	514.8	1	12.5	30.5	5
Calcined at 400 °C	444.8	517.2	1.3	3.6	1.5	0.3
Calcined at 550 °C	444.2	517.1	1.2	2.5	1.9	0

O and C are the oxide- and carbonate-related components in the O1*s* and C1*s* complex peak, respectively, containing that of the contamination CO_2 in the atmosphere.

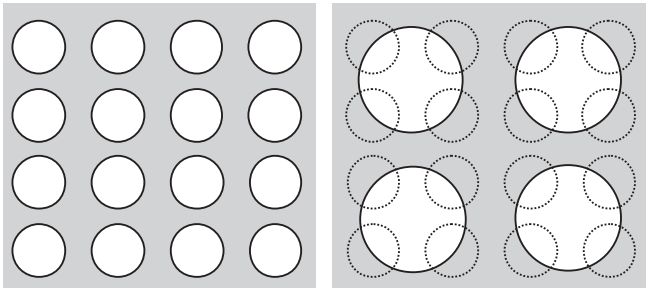

Fig. 8. Schematic pore structures of the films obtained under lower (a) and higher (b) calcination temperature.

For our experiments, all the films displayed in Fig. 1 were formed by a single application of the precursor solution followed by an annealing for 4 h at a given temperature, with the same heating-up rate of 3 °C/min. If we want to get the small pore and well-crystallized $InVO_4$ films, we can calcine the precursor film at a relatively low temperature for a longer time to decompose the organic components, and then crystallize the film at a relatively high temperature. From the SEM results (Fig. 1), we can find that there are some open pores on the films obtained at a low temperature (450 °C), and then it is possible to decompose the organic components at a low temperature for a long time. From the TG and DTA curves (Fig. 5), the last stage of the weight loss of the precursor begins at 410 °C, so it is necessary to decompose the organic components at a temperature above 410 °C.

3.4. Optical and photocatalytic properties

Fig. 9 shows the UV–visible light transmittance spectra of the as-prepared films. The fringes are the result of interference between radiation from the air-film and film-substrate interfaces. The presence of these fringes indicates that the films are quite uniform in thickness, as nonuniform thickness would destroy all interference effects resulting in a smooth transmittance curve. At lower calcination temperature, the transmittance is lower, owing to the residue of the free carbon without liberation from the film. With the increase of the calcination temperature, the transmittance increased.

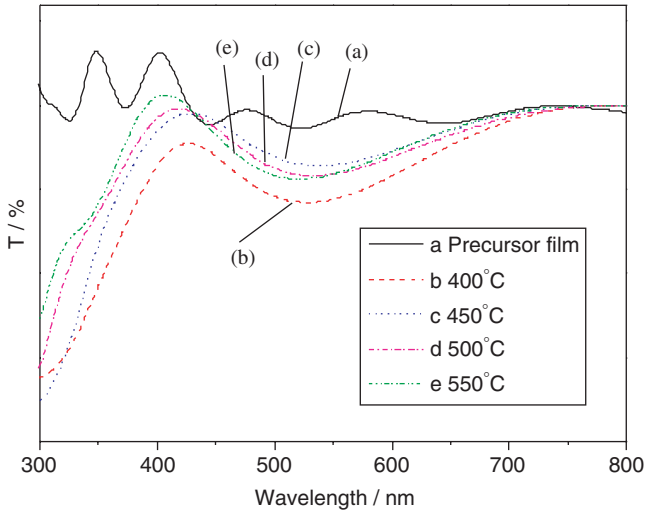

Fig. 9. UV–VIS transmittance spectra of the precursor film (a) and the $InVO_4$ films obtained under different calcination temperature: 400 °C (b), 450 °C (c), 500 °C (d), 550 °C (e).

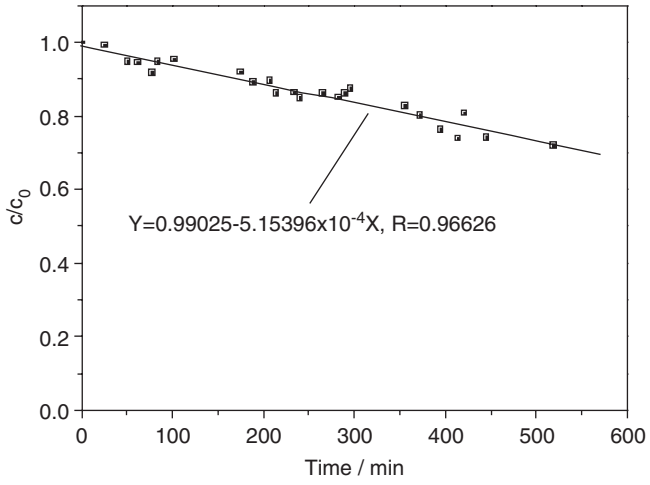

Fig. 10. Photocatalytic degradation of formaldehyde on the surface of a six layer $InVO_4$ film under visible light irradiation ($\lambda > 400$ nm, 31 mW cm^{-1}).

The photocatalytic activity of $InVO_4$ films under visible light irradiation was evaluated by the photocurrent and the photodegradation of gaseous formaldehyde.

Fig. 10 shows the result of the photodegradation of gaseous formaldehyde on the six layer porous $InVO_4$ films, where C is the concentration of formaldehyde at the irradiation time t and C_0 is the concentration in the adsorption equilibrium on $InVO_4$ before irradiation (about 430 ppm). The result indicated that the concentration of gaseous formaldehyde reduced from 430 to 310 ppm in 520 min. C/C_0 linearly decreases with the increase of irradiation time. Namely, the photocatalytic reaction of gaseous formaldehyde on the surface of $InVO_4$ films can be considered a zero grade reaction.

Photoelectrochemical experiments were also conducted in a propylene carbonate solution containing 1 mol L^{-1} $LiClO_4$. An anodic photocurrent of significant magnitude (sub-μA cm^{-2}) was observed when the six layer porous $InVO_4$ film electrode was irradiated with visible light ($\lambda > 400$ nm) at 0 V (Fig. 11).

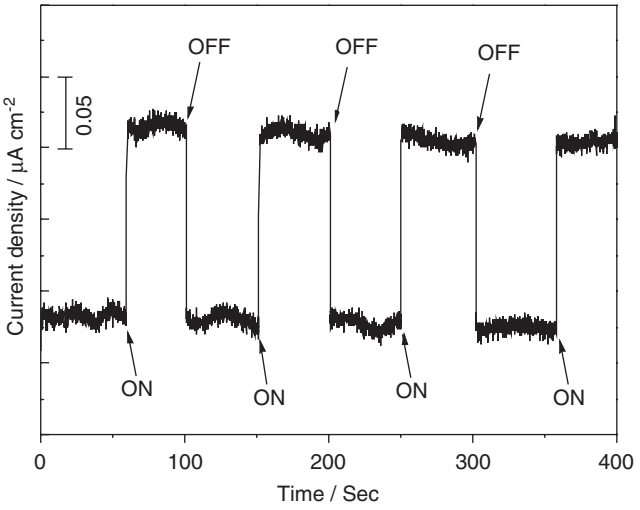

Fig. 11. Photocurrent generation from the 6 layer films of $InVO_4$/ITO electrode at 0 V under visible light irradiation ($\lambda > 400$ nm).

In our experiments, the efficient area of $InVO_4$ films is about 4 cm^2. The thickness of six layer films is about 600 nm. The density of the orthorhombic crystalline stable $InVO_4$-III phase is 4.7 g cm^{-3} [36]. The amount of $InVO_4$ in the six layer dense films is only about 1.128 mg. For the porous films, the amount is far smaller than this value. So it is possible to improve the photocatalytic activity by modifying the structure of the films, such as increasing the thickness. The further investigations are now ongoing.

3.5. Electrochemical properties

The porous structure and the crystal structure of the films have great effects on the film properties. Denis et al. [23] have found that the amorphous $InVO_4$ powders exhibit a better charging/discharging capacity and smaller charge capacity fade with cycling than the crystalline counterparts. Santato et al. [3] have found that the mesoporous WO_3 films can be penetrated by the electrolyte down to the back contact to form high-surface-area semiconductor/liquid junctions.

In order to evaluate the electrochemical properties of the porous $InVO_4$ films, they were submitted to cyclic voltammetry in a solution of 1 M $LiClO_4$ in propylene carbonate. The cyclovoltammetric curves of the as-prepared films were shown in Fig. 12. At 400 °C, the surface of the film is uniform and has no pores, and still has some residue organic components in the film, which lead to the lower charge capacity. Owing to the amorphous phase of $InVO_4$ films and their porous structure, CV curve of the film obtained at 450 °C shows the highest charge densities and one anodic peak at 0.22 V. After crystallization (at 500

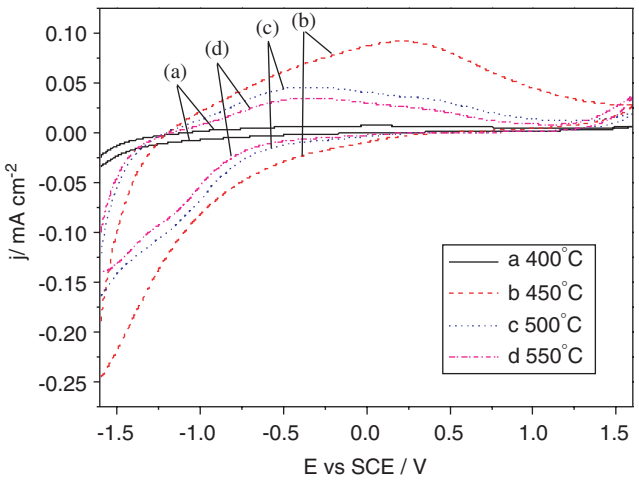

Fig. 12. CV response of the as-prepared films obtained under different calcination temperature: 400 °C (a), 450 °C (b), 500 °C (c), 550 °C (d).

and 550 °C), with increase of the calcination temperature, the pore size increases, and leads to the smaller surface-area semiconductor/liquid junctions, and then the lower charge capacity, with one cathodic peak at −1.14 V and two anodic peaks at −0.35 and 0.42 V. Our results show a similar phenomena as those in the literatures. By changing the crystal structure and the pore structure, it is easy to modify the properties of the films.

4. Conclusions

We have successfully prepared the porous $InVO_4$ films on ITO substrate by direct pyrolysis of the amorphous complex oxide. The amorphous complex oxide is produced by the complexation between diethylenetriaminepentaacetic acid and the cheap inorganic metal salts or metal oxides. The films with crystallographically orientated and the pure orthorhombic $InVO_4$ can be obtained at high temperature (500 and 550 °C). The pore size can be easily modified by changing the calcination temperature. The porous $InVO_4$ films have shown the photocatalytic activity for photodegradation of gaseous formaldehyde, and can generate photocurrent under visible light irradiation ($\lambda > 400$ nm). We have established a clear correlation between the crystallinity and the pore structure of the $InVO_4$ films and their electrochemical properties. This method has a potential use in the preparation of porous films of other complex oxide. And such porous films of the complex oxide have the potential applications in catalysis, photoelectrodes, photocatalysts, gas sensors, electrochromic materials, lithium ion batteries, and so on.

Acknowledgments

This work was partly supported by the Chinese National Science Foundation (20433010), Trans-Century Training Program Foundation for the Talents by the Ministry of Education, P.R.C., the Excellent Young Teacher Program of MOE, P.R.C., and the China Postdoctoral Science Foundation.

References

[1] A. Taguchi, F. Schuth, Micropor. Mesopor. Mat. 77 (2005) 1.
[2] B. O'Regan, M. Gratzel, Nature 353 (1991) 737.
[3] C. Santato, M. Ulmann, J. Augustynski, Adv. Mater. 13 (2001) 511.
[4] C. Santato, M. Odziemkowski, M. Ulmann, J. Augustynski, J. Am. Chem. Soc. 123 (2001) 10639.
[5] L. Zhang, Y.F. Zhu, Y. He, W. Li, H.B. Sun, Appl. Catal. B 40 (2003) 287.
[6] J.C. Yu, X.C. Wang, X.Z. Fu, Chem. Mater. 16 (2004) 1523.
[7] B. Yuliarto, H.S. Zhou, T. Yamada, I. Honma, Y. Katsumura, M. Ichihara, Anal. Chem. 76 (2004) 6719.
[8] Y. Shimizu, T. Hyodo, M. Egashira, Catal. Surv. Asia 8 (2004) 127.
[9] M.T. Moller, S. Asaftei, D. Corr, M. Ryan, L. Walder, Adv. Mater. 16 (2004) 1558.
[10] W. Cheng, E. Baudrin, B. Dunn, J.I. Zink, J. Mater. Chem. 11 (2001) 92.
[11] H.S. Zhou, D.L. Li, M. Hibino, I. Honma, Angew. Chem. Int. Edit. 44 (2005) 797.
[12] A. Attia, M. Zukalova, J. Rathousky, A. Zukal, L. Kavan, J. Solid State Electr. 9 (2005) 138.
[13] V.V. Guliants, M.A. Carreon, Y.S. Lin, J. Membrane Sci. 235 (2004) 53.
[14] F. Schuth, Chem. Mater. 13 (2001) 3184.
[15] J.Y. Ying, C.P. Mehnert, M.S. Wong, Angew. Chem. Int. Ed. 38 (1999) 56.
[16] A. Sayari, P. Liu, Micropor. Mater. 12 (1997) 149.
[17] D. Zhao, J. Feng, Q.S. Huo, N. Melosh, G.H. Fredrickson, B.F. Chmelka, G.D. Stucky, Science 279 (1998) 548.
[18] P. Yang, D. Zhao, D.I. Margolese, B.F. Chmelka, G.D. Stucky, Nature 396 (1998) 152.
[19] B. Tian, X. Liu, B. Tu, C. Yu, J. Fan, L. Wang, S. Xie, G. Stucky, D. Zhao, Nat. Mater. 2 (2003) 159.
[20] P. Jiang, J. Cizeron, J.F. Bertone, V.L. Colvin, J. Am. Chem. Soc. 121 (1999) 7957.
[21] G. Subramania, K. Constant, R. Biswas, M.M. Sigalas, K.M. Ho, Appl. Phys. Lett. 74 (1999) 3933.
[22] P.N. Bartlett, J.J. Baumberg, P.R. Birkin, M.A. Ghanem, M.C. Netti, Chem. Mater. 14 (2002) 2199.
[23] S. Denis, E. Baudrin, M. Touboul, J.M. Tarascon, J. Electrochem. Soc. 144 (1997) 4099.
[24] A.S. Vuk, B. Orel, G. Drazic, J. Solid State Electr. 5 (2000) 437.
[25] M. Oshikiri, M. Boero, J.H. Ye, Z.G. Zou, G. Kido, J. Chem. Phys. 117 (2002) 7313.
[26] J. Ye, Z. Zou, H. Arakawa, M. Oshikiri, M. Shimoda, A. Matsushita, T. Shishido, J. Photochem. Photobio. A 148 (2002) 79.
[27] J. Ye, Z. Zou, M. Oshikiri, A. Matsushita, M. Shimoda, M. Imai, T. Shishido, Chem. Phys. Lett. 356 (2002) 221.
[28] M. Oshikiri, M. Boero, J. Ye, F. Aryasetiawan, G. Kido, Thin Solid Films 445 (2003) 168.
[29] A.S. Vuk, U.O. Krasovec, B. Orel, P. Colomban, J. Electrochem. Soc. 148 (2001) H49.
[30] B. Orel, A.S. Vuk, U.O. Krasovec, G. Drazic, Electrochim. Acta 46 (2001) 2059.
[31] F. Artuso, F. Decker, A. Krasilnikova, M. Liberatore, A. Lourenco, E. Masetti, A. Pennisi, F. Simone, Chem. Mater. 14 (2002) 636.
[32] H. Wullens, D. Leroy, M. Devillers, Int. J. Inorganic Mater. 3 (2001) 309.
[33] C. Zhang, L. Wang, L.P. Cui, Y.F. Zhu, J. Crystal Growth 255 (2003) 317.
[34] Y.F. Zhu, R.Q. Tan, J. Feng, S.S. Ji, L.L. Cao, Appl. Catal. A 209 (2001) 71.
[35] H. Wang, Y.F. Zhu, P. Liu, W.Q. Yao, J. Mater. Sci. 38 (2003) 1939.

[36] M. Touboul, P. Toledano, Acta Crystallogr. B 36 (1980) 240.
[37] E.J. Baran, M.E. Escobar, Spectrochim. Acta 41A (1985) 415.
[38] M. Touboul, A. Popot, J. Therm. Anal. 31 (1986) 117.
[39] N. Cimino, F. Artuso, F. Decker, B. Orel, A.S. Vuk, R. Zanoni, Solid State Ionics 165 (2003) 89.
[40] A. Surca, B. Orel, G. Drazic, B. Pihlar, J. Electrochem. Soc. 146 (1999) 232.
[41] C.N. de Carvalho, A.B. do Rego, A. Amaral, P. Brogueira, G. Lavareda, Surf. Coat. Tech. 124 (2000) 70.
[42] K. Nakanishi, J. Porous. Mater. 4 (1997) 67.